remote sensing

MDPI

Letter

A Sensitivity Study of the 4.8 μm Carbon Dioxide Absorption Band in the MWIR Spectral Range

Vito Romaniello *, Claudia Spinetti, Malvina Silvestri and Maria Fabrizia Buongiorno

Istituto Nazionale di Geofisica e Vulcanologia, Roma 00143, Italy; claudia.spinetti@ingv.it (C.S.); malvina.silvestri@ingv.it (M.S.); fabrizia.buongiorno@ingv.it (M.F.B.)

* Correspondence: vito.romaniello@ingv.it

Received: 29 October 2019; Accepted: 27 December 2019; Published: 3 January 2020

Abstract: The measurements of gas concentrations in the atmosphere are recently developed thanks to the availability of gases absorbing spectral channels in space sensors and strictly depending on the instrument performances. In particular, measuring the sources of carbon dioxide is of high interest to know the distribution, both spatial and vertical, of this greenhouse gas and quantify the natural/anthropogenic sources. The present study aims to understand the sensitivity of the CO_2 absorption band at 4.8 μm to possibly detect and measure the spatial distribution of emissions from point sources (i.e., degassing volcanic plumes, fires, and industrial emissions). With the aim to define the characteristics of future multispectral imaging space radiometers, the performance of the CO_2 4.8 μm absorption band was investigated. Simulations of the "Top of Atmosphere" (TOA) radiance have been performed by using real input data to reproduce realistic scenarios on a volcanic high elevation point source (>2 km): actual atmospheric background of CO_2 (~400 ppm) and vertical atmospheric profiles of pressure, temperature, and humidity obtained from probe balloons. The sensitivity of the channel to the CO_2 concentration has been analyzed also varying surface temperatures as environmental conditions from standard to high temperature. Furthermore, response functions of operational imaging sensors in the middle wave infrared spectral region were used. The channel width values of 0.15 μm and 0.30 μm were tested in order to find changes in the gas concentration. Simulations provide results about the sensitivity necessary to appreciate carbon dioxide concentration changes considering a target variation of 10 ppm in gas column concentration. Moreover, the results show the strong dependence of at-sensor radiance on the surface temperature: radiances sharply increase, from 1 $Wm^{-2}sr^{-1}\mu m^{-1}$ (in the "standard condition") to >1200 $Wm^{-2}sr^{-1}\mu m^{-1}$ (in the warmest case) when temperatures increase from 300 to 1000 K. The highest sensitivity has been obtained considering the channel width equal to 0.15 μm with noise equivalent delta temperature (NEDT) values in the range from 0.045 to 0.56 K at surface temperatures ranging from 300 to 1000 K.

Keywords: carbon dioxide; multispectral sensor; earth observation; satellite; MWIR

1. Introduction

The evidence of increasing Earth surface temperature in the last decades [1] is posing important questions about the causes and the influence of human activities on it. The greenhouse gases play a crucial role in the global warming trend [2] and their characterization is increasingly necessary. The individuation and quantification of gases point sources are pivotal to better understand the anthropogenic and natural origins. The measurements of gas concentrations taken remotely, with the identification of their spatial distribution, are developed thanks to the availability of the gases absorbing spectral channels in the sensors carried on satellite or airborne platforms. Atmospheric CO_2 total columns can be measured by sensors acquiring spectra in the CO_2 absorption bands at 1.6 μm and 2.0 μm in the short-wave infrared (SWIR) spectral region, at 4 μm in the midwave infrared (MWIR),

and at 15 μm in the thermal infrared (TIR) spectral regions. Figure 1 shows absorption bands in the SWIR–MWIR spectral range.

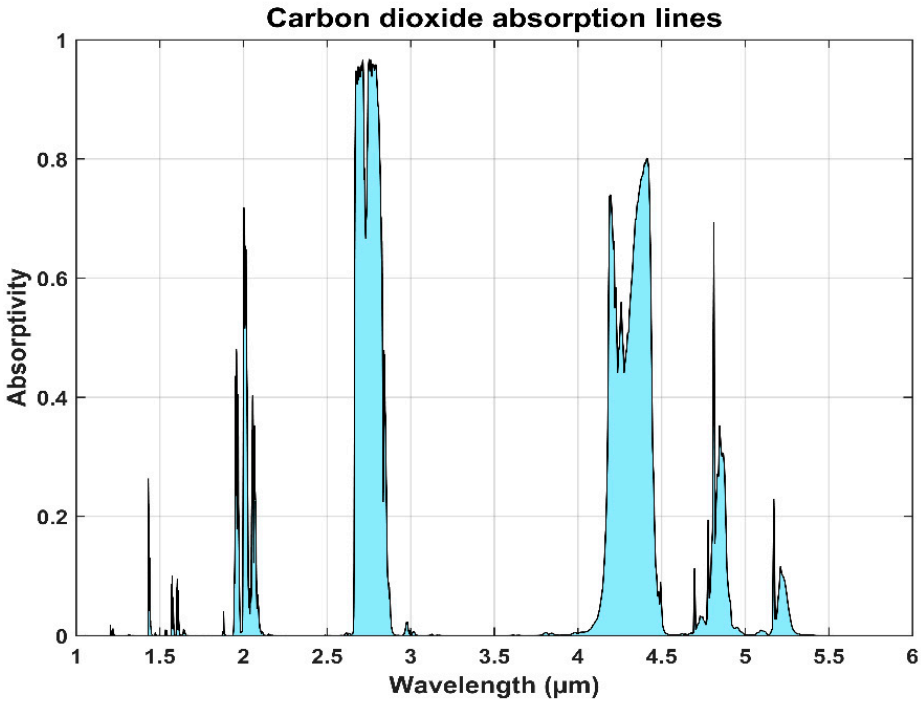

Figure 1. Carbon dioxide absorption bands in the SWIR–MWIR spectral range.

TIR has the advantage of providing day and night continuous measurements. The first retrieval of column averaged mixing ratio of CO_2 in dry air (XCO2) has been from the infrared sounder TOVS (TIROS Operational Vertical Sounder) [3,4] demonstrating the limited capability to constrain CO_2 sources and sinks [5]. The high-resolution infrared sounders, such as the AIRS (Atmospheric InfraRed Sounder) [6] and IASI (Infrared Atmospheric Sounding Interferometer) [7], were shown to attain a substantial gain of information mostly due to their broader spectral coverage and finer resolution. Therefore, the XCO2 retrieved from IASI measurements reached the precision of 2 ppm for a 5° × 5° spatial resolution on a monthly time scale [7–9].

CO_2 absorption bands in the SWIR spectral range have the advantage of being sensitive down to the lowermost layers of the atmosphere, which contain information about surface fluxes useful for identification of CO_2 sources and sinks. In this spectral region, XCO2 has been measured by SCIAMACHY (2002–2012) [10], TANSO-FTS (2009–present) [11], OCO-2 (2014–present) [12–14], TanSAT (2016 to present) [15], and the recent OCO-3 on board ISS [16]. The OCO-2 mission provides measurements up to now from space at higher spatial resolution of 1.30 km × 2.25 km reaching the 0.5 ppm precision for XCO2 necessary to identify CO_2 gradients across large urban areas [17].

Instead, the CO_2 absorption bands in the MWIR region lack studies in the literature, although this band is particularly suitable for remote sensing due to the position in an atmospheric window [18] on the MWIR spectral region. Indeed, this spectral region has several advantages: it is characterized by low values of Earth reflectance leading to low backscattering effects. Moreover, the radiance emitted by the Earth in this spectral range allows continuous acquisitions during day and night. Finally, we expect a measurable amount of energy at the sensor, independently from the pixel size, from high-temperature events due to the fact that Wien's displacement law determines the temperature at which the maximum energy will radiate and the 3–5 μm range corresponds to the radiant energy peak for temperatures of 600 K and greater (see Figure 2), which are associated with fires, lava flows, and other hot features [19].

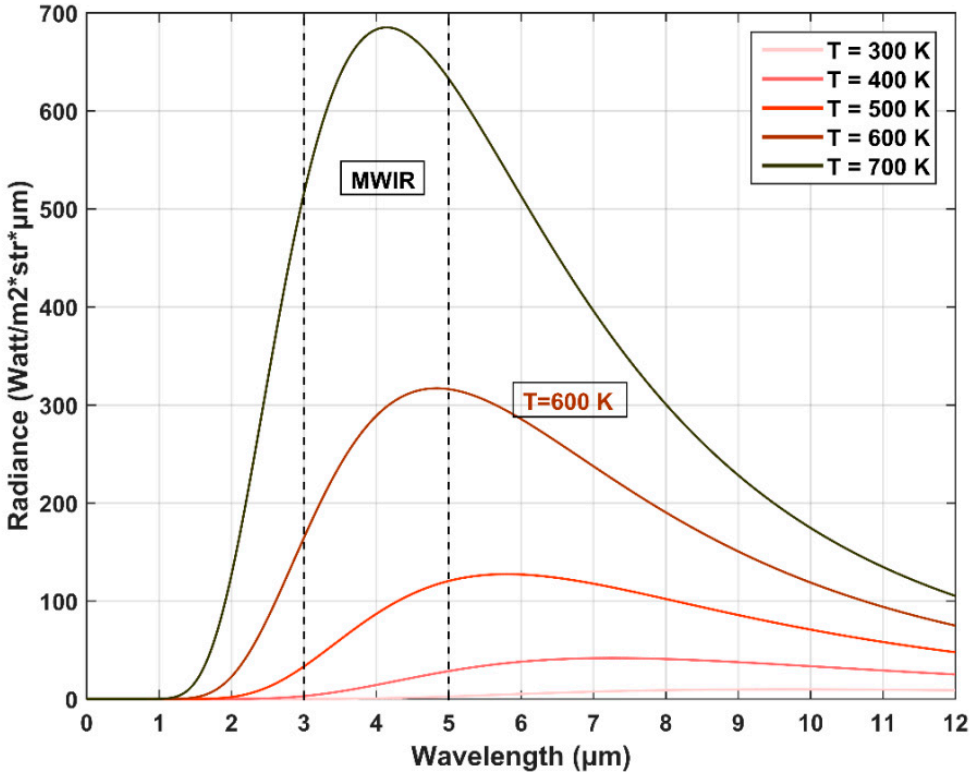

Figure 2. Radiation emitted from blackbodies at T = 300, 400, 500, 600, 700 K (Wien's displacement law).

The scope of the present study is to understand the capability of the absorption band at 4.8 µm to detect and measure the spatial distribution of CO_2 emissions from point sources as degassing volcanic plumes [20], fires [21], and industrial emissions [22]. This study can be useful to define the characteristics of multispectral imaging space radiometers to be employed in future space missions whose applications include greenhouse gas observations. The possibility of detecting CO_2 point sources is related to both the sensitivity and the spatial resolution of the sensor itself.

We expect several advantages in using the 4.8 µm absorption band. First of all, the band is located in an atmospheric window, just before the strong water absorption bands in the range 5–8 µm [18,23]. The 4.8 µm band has absorptivity comparable to the SWIR band at 2 µm, thus suggesting the amount of energy reaching a space sensor is sufficient to be a useful band for measuring the CO_2 amount in the atmosphere, whereas the 4.2–4.4 µm absorption band has absorptivity close to one, so the energy reaching a space sensor is too low.

The performance of the 4.8 µm absorption band in retrieving CO_2 concentrations was analyzed by means of the MODerate resolution atmospheric TRANsmission (MODTRAN) radiative transfer model [24]. Specifically, the role of surface temperatures below gas emissions was investigated; the width of the channel was also considered in the analyses with the aim to understand its influence on the sensitivity of multispectral space sensors.

2. Simulations of CO_2 Absorption Band at 4.8 µm

In order to simulate the radiance at the satellite sensor, in the MWIR spectral region, the MODTRAN computer code [24], version 4, was used. The MODTRAN transfer model is based on the radiative transfer Equation (1). The at-sensor measured radiance in the thermal spectral region is a combination of three primary terms: the Earth-emitted radiance, reflected downwelling radiance (thermal + solar components), and total atmospheric path radiance (thermal + solar components):

$$L_{obs}(\lambda,\theta) = \tau_\lambda(\theta)\Big[\epsilon_\lambda B(\lambda,T_s) + \rho_\lambda\Big(L_s^{\downarrow}(\lambda,\theta) + L_t^{\downarrow}(\lambda,\theta)\Big)\Big] + L_t^{\uparrow}(\lambda,\theta) + L_s^{\uparrow}(\lambda,\theta) \quad (1)$$

where $L_{obs}(\lambda, \theta)$ is the at-sensor radiance, λ is wavelength, θ is the satellite viewing angle, ϵ_λ is the surface emissivity, ρ_λ is surface reflectance, $B(\lambda, T_s)$ is the Planck function describing radiance emitted at surface temperature, T_s, $L_s^{\downarrow}$ is the total (diffuse and direct) downwelling solar radiance, $L_t^{\downarrow}$ is the downwelling thermal irradiance, $\tau_\lambda(\theta)$ is the atmospheric transmittance, $L_s^{\uparrow}(\lambda,\ \theta)$ is the upward path solar radiance, and $L_t^{\uparrow}(\lambda,\ \theta)$ is the upward thermal path radiance reaching the sensor.

2.1. MODTRAN General Setup and Performed Runs

In this work, the model setup considered was the default [24], assuming 37 not equispaced atmospheric vertical levels from 2 to 100 km as representative of an elevated CO_2 emitting point source in a volcanic or mountain area with elevations >2 km (Figure 3d). The runs were operated using a real scenario with atmospheric profiles of pressure, temperature and water obtained from a balloon sounding on Trapani (Sicily, Italy). These profiles (Figure 3a–c) were chosen following the criteria of the representativeness of the midlatitude autumn in a stable atmospheric day on Sicily island where Mount Etna volcano (3330 m a.s.l.) is located. Quiescent emissions from Mount Etna's summit are a high natural point source of CO_2 [25]. Table 1 reports the main parameters used as input for the MODTRAN simulations. The surface albedo has been set considering homogeneous lava surface [26].

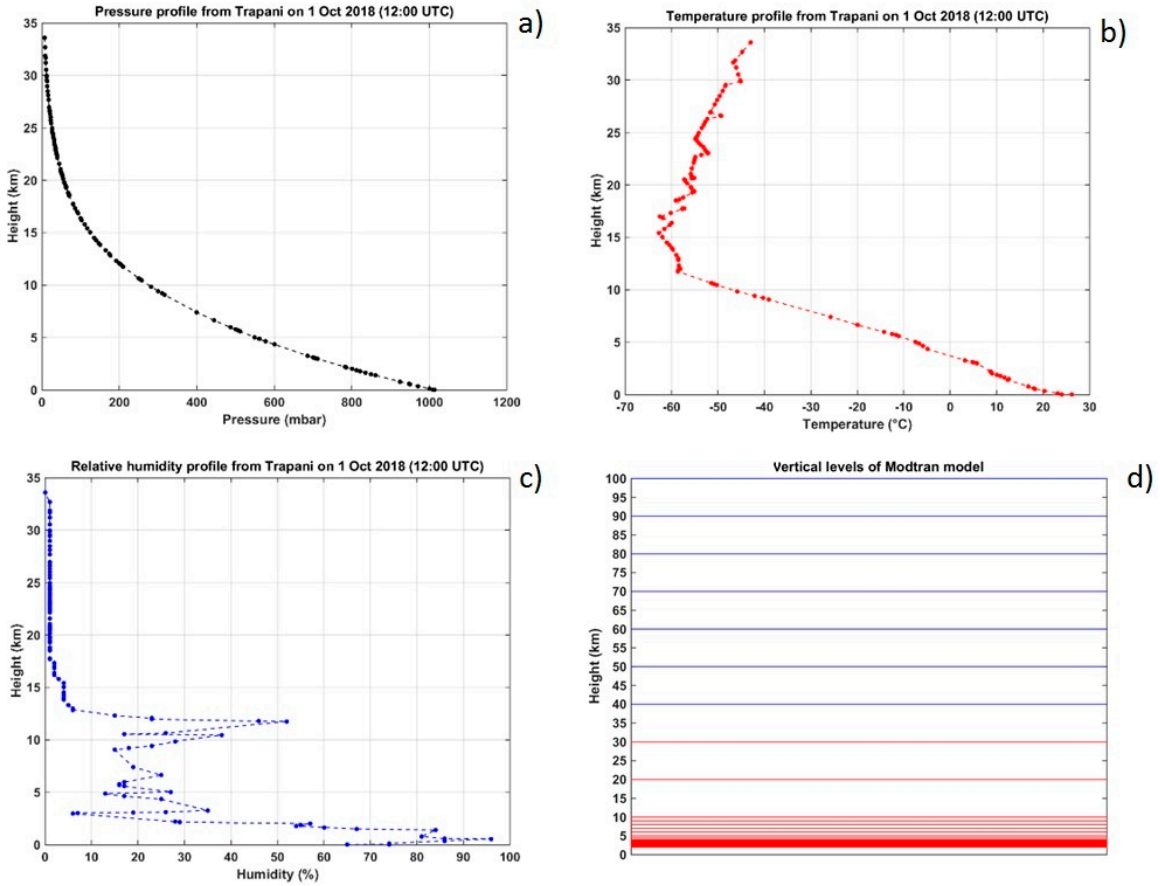

Figure 3. Atmospheric profiles of pressure (**a**), temperature (**b**), and humidity (**c**) obtained from a balloon sounding on Trapani (Sicily, Italy) and simulated vertical levels (**d**).

Table 1. Input Parameters for MODTRAN Simulations in "Standard Conditions".

Input Parameter	Value
Spectral range	MWIR: 3–6 μm
Atmospheric profiles of temperature, pressure, and humidity	Balloon sounding on Trapani (1 October 2018)
Surface temperature	300 K
CO_2 concentration	400 ppm
Albedo	0.10
Altitude of the first layer	2 km
Altitude of the last layer	600 km
Number of vertical levels	37
Aerosol	NO

In order to evaluate the sensitivity of the 4.8 μm channel to CO_2 changes, several runs of the model were carried out considering incremental CO_2 concentrations in atmosphere and temperatures at the ground. The CO_2 concentrations were considered in the range 0–1000 ppm at intervals of 200 ppm, in a first step fixing the surface temperature at 300 K (Figure 4) and in a second step increasing the surface temperatures from 300 K to 1000 K at intervals of 100 K. So, a total of 48 runs were performed to analyze the sensitivity as a function of CO_2 concentration and of ground temperatures that are spread in a wide range in the case of a high-temperature event (HTE).

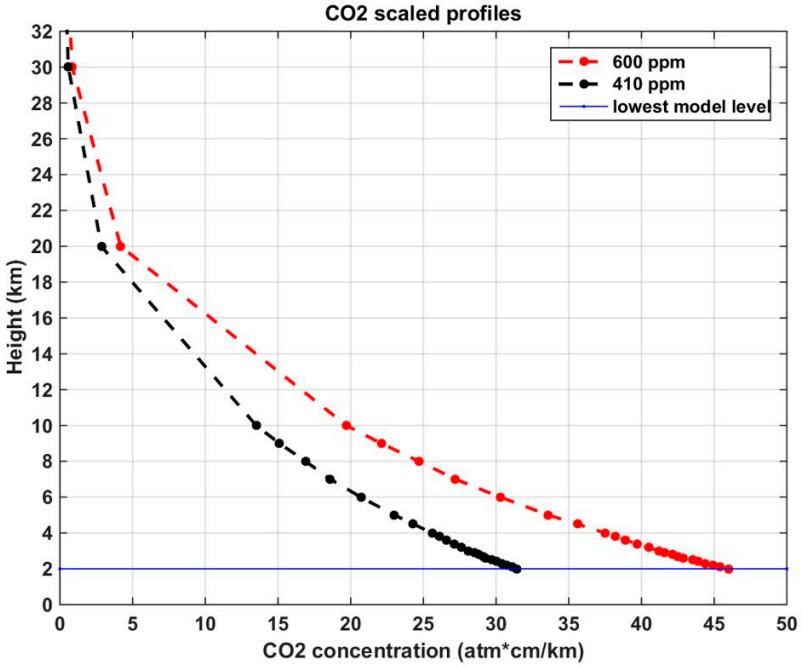

Figure 4. MODTRAN CO_2 vertical profiles.

2.2. Response Functions and Convolution of Radiances

A main objective of the study is to assess the usability of the channel for multispectral imaging space radiometers. So, with the aim of evaluating the response of satellite sensors to incoming radiances, it is necessary to consider the characteristics of the sensor and specifically the response function for the 4.8 μm absorption band. Since the current multispectral imaging space radiometers with detectors in the MWIR do not employ this channel (e.g., MODIS and AVHRR), we considered typical response functions of operational sensors carried on aircrafts; in particular, the response function of the MASTER (Modis ASTER) airborne simulator [27,28] was taken into account. Then, the response function was adapted for our needs, maintaining the same shape and changing the full width half maximum

(FWHM) in order to test two different solutions: two response functions were considered with FWHM equal to 0.15 and 0.30 μm (see Figure 5).

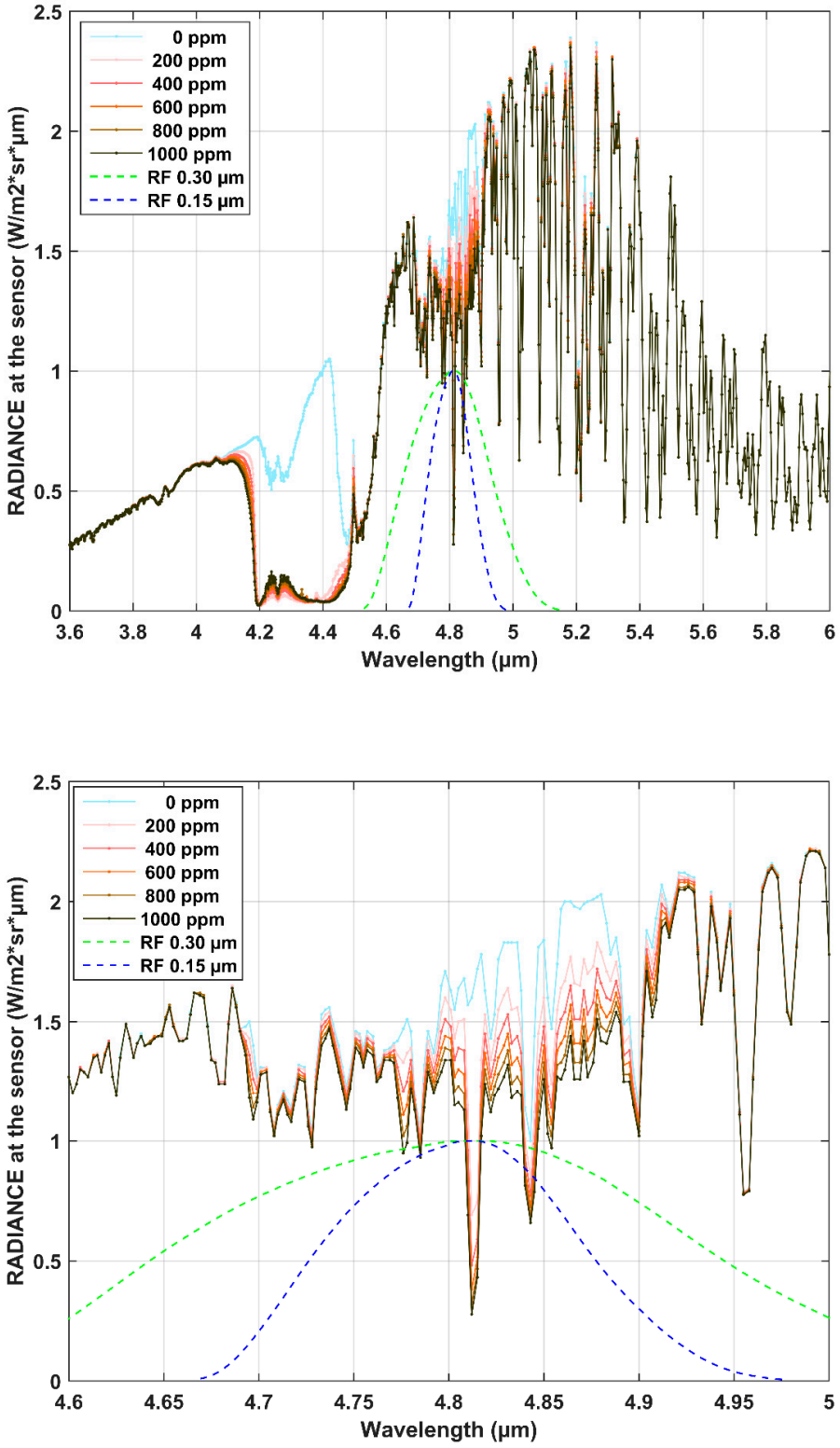

Figure 5. Simulated TOA radiances for several CO_2 concentrations in the MWIR spectral range; the considered response functions are depicted (dotted green line: FWHM = 0.30 μm; dotted blue line: FWHM = 0.15 μm). A zoom on the absorption band is also reported in the bottom.

3. Simulation Results

As described in Section 2.1, a total number of 48 runs was performed; for each considered surface temperature, the dependence of the radiance on the CO_2 concentration was analyzed. Figure 5 shows the simulated radiances at the top of atmosphere (TOA), with a fixed surface temperature of 300 K (standard condition), for CO_2 concentrations ranging from 0 to 1000 ppm in the lower troposphere. The response functions derived from the MASTER instrument and used in the present work are also reported in Figure 5 (green and blue dotted lines). The maximum CO_2 concentrations of 1000 ppm generated a decrease of about 1 $Wm^{-2}sr^{-1}\mu m^{-1}$ in the radiance simulations (Figure 5 zoom).

The strong water absorption started from about 5 μm and could have partially affected the CO_2 band; so, a large response function could have included the contribution of the water in the atmosphere. The sensitivity of the absorption band to increasing concentrations of carbon dioxide is also highlighted in Figure 5: the radiance at the sensor decreased, in the range 4.7–4.9 μm, with increasing gas concentration. Moreover, the very strong CO_2 band in the spectral range 4.2–4.4 μm [29] was unusable due to the strong absorption of the remote signal at atmospheric background conditions (~400 ppm).

3.1. Radiance as Function of CO_2 and T

In order to analyze the behavior of the channel at 4.8 μm as a function of CO_2 concentrations and surface temperatures, TOA simulated radiances were convolved on response functions described above. In the following analyses, a function with FWHM = 0.15 μm was firstly considered, since a narrower response function is less affected by the presence of water in the atmosphere; furthermore, this is the typical width employed in operational sensors carried on aircrafts such as the MASTER airborne simulator. Once the surface temperature was fixed, the TOA radiance was convolved for several CO_2 concentrations ranging from 0 to 1000 ppm; the dependence of radiance on the gas concentration could be thus obtained. Moreover, this function was derived for different temperatures at ground, ranging from 300 to 1000 K, and results are reported in Figure 6; for a better representation, the logarithmic scale is used for radiance values. As we expected, the radiance sharply increased with increasing temperatures, reaching values more than 1200 $Wm^{-2}sr^{-1}\mu m^{-1}$ in the warmest case. Considering that typical values of radiance are 1–2 $Wm^{-2}sr^{-1}\mu m^{-1}$ in the "standard condition", the surface temperature plays a crucial role in determining the total energy retrieved by sensors.

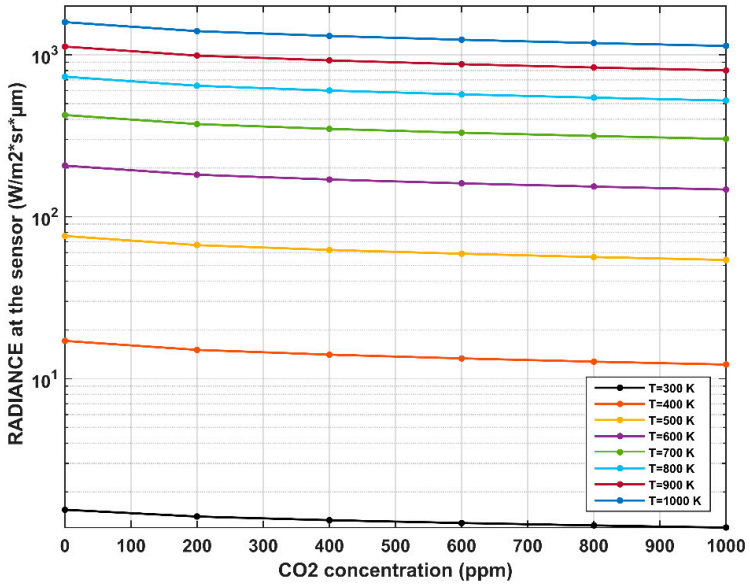

Figure 6. Simulated TOA radiances (in logarithmic scale), after the convolution considering FWHM = 0.15 μm, as function of CO_2 concentrations for several surface temperatures.

A nearest-neighbor interpolation technique was applied to the simulated radiances with the aim to obtain a continuous function of the two parameters, CO_2 concentration and temperature. The result is a three-dimensional function, describing the behavior of the 4.8 µm absorption band (Figure 7).

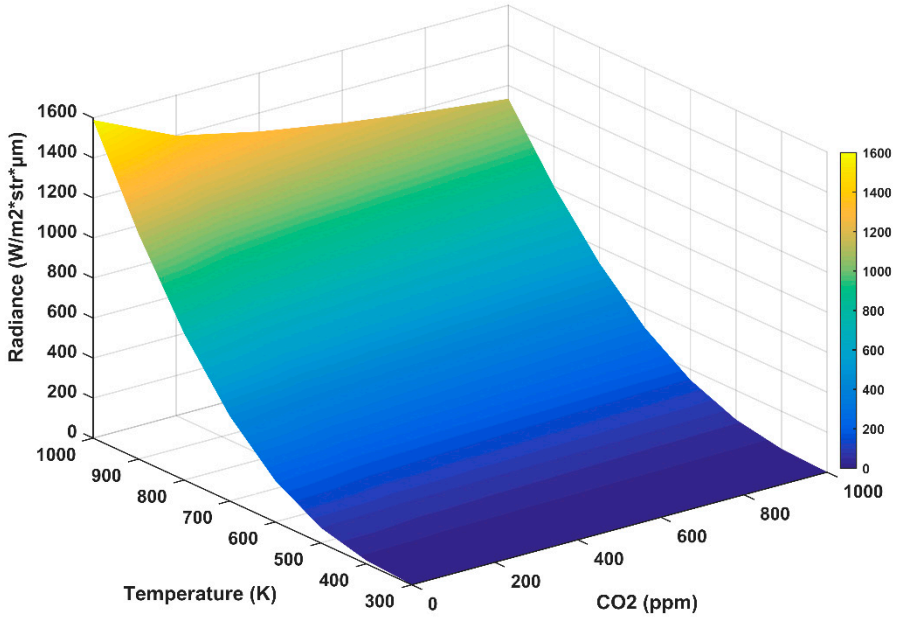

Figure 7. Simulated at-sensor radiances (interpolated), after the convolution considering FWHM = 0.15 µm, as function of CO_2 concentration and surface temperature.

3.2. Sensitivity Analyses: Noise Equivalent Delta Temperature and Signal-to-Noise Ratio

The analysis of at-sensor radiance as a function of CO_2 concentration and surface temperature is propaedeutic for calculating and defining characteristics for future space sensors employing the considered spectral channel. In particular, the required accuracy of MWIR sensors is a fundamental parameter which allows detecting and distinguishing gas emission phenomena. So, sensitivity analyses are useful to answer the question: what is the instrumental accuracy necessary to observe a variation of CO_2 concentration in the atmosphere by using the channel at 4.8 µm? Considering the signal-to-noise ratio definition (Equation (2)), minimum conditions to observe gas variations can be defined.

$$SNR_\lambda = \frac{R_\lambda}{NedR} \geq \frac{R_\lambda}{\Delta R_\lambda^m} \tag{2}$$

where SNR_λ = signal-to-noise ratio, R_λ = radiance at the sensor, NedR = noise equivalent delta radiance, ΔR_λ^m = delta radiance value (signature to measure).

Then, in order to detect the radiance changes due to gas concentration changes, the noise equivalent delta radiance of the sensor must be less than the delta radiance value (Equation (3)).

$$NedR \leq \Delta R_\lambda^m \tag{3}$$

Now, we can calculate the decreasing rate of at-sensor radiance for increasing CO_2 concentrations (see Figure 6) and derive the angular coefficient under the first approximation of linear behavior. In the following, we consider, as signature to measure, the delta radiance value due to a CO_2 increasing of 10 ppm in the entire atmospheric column. This allows calculating sensitivity parameters for each temperature considered in the MODTRAN simulations (Table 2). The noise equivalent delta temperature (NEDT) parameter was derived from the NedR by means of the Planck law; the considered temperatures for black body emissions are reported in Table 2.

Table 2. Sensitivity Parameters for Several Surface Temperatures Considering a Variation of 10 ppm with a FHWM = 0.15 μm.

Parameters\Temp.	300 K	400 K	500 K	600 K	700 K	800 K	900 K	1000 K
Angular coefficient ($Wm^{-2}sr^{-1}\mu m^{-1}ppm^{-1}$)	–0.0033	–0.046	–0.21	–0.56	–1.15	–1.98	–3.03	–4.29
NedR ($mWm^{-2}sr^{-1}\mu m^{-1}$)	<3.3	<46	<210	<560	<1150	<1980	<3030	<4290
NEDT (K)	<0.045	<0.095	<0.15	<0.21	<0.28	<0.36	<0.45	<0.56
SNR	>405.5	>306.0	>297.0	>303.1	>303.1	>303.6	>304.6	>304.6

As we expected, the NEDT increased with increasing temperatures at the ground because of greater energy received by the instrument. A higher sensitivity of the sensor is required for lower temperatures to detect changes in gas concentration. A lower sensitivity is instead necessary in case of HTEs; considering, for example, a surface temperature of 600 K in the radiative transfer model, the NEDT must be less than 0.21 K in order to detect a variation of 10 ppm in the CO_2 concentration.

The FWHM parameter of the sensor response function is also crucial for retrieving changes in gas concentration. All calculations above were performed considering a FWHM = 0.15 μm; it is useful to evaluate the impact of a wider/narrower response function. Following the characteristics of operative multispectral space sensors, a FWHM = 0.30 μm was considered; the NEDT values were recalculated and are reported in Figure 8. The NEDT was greater, for all ground temperatures, in the case of 0.15 μm: the results indicate the best performances by using the narrower response function. This is probably due also to the closest N_2 absorption band that can influence the larger channel.

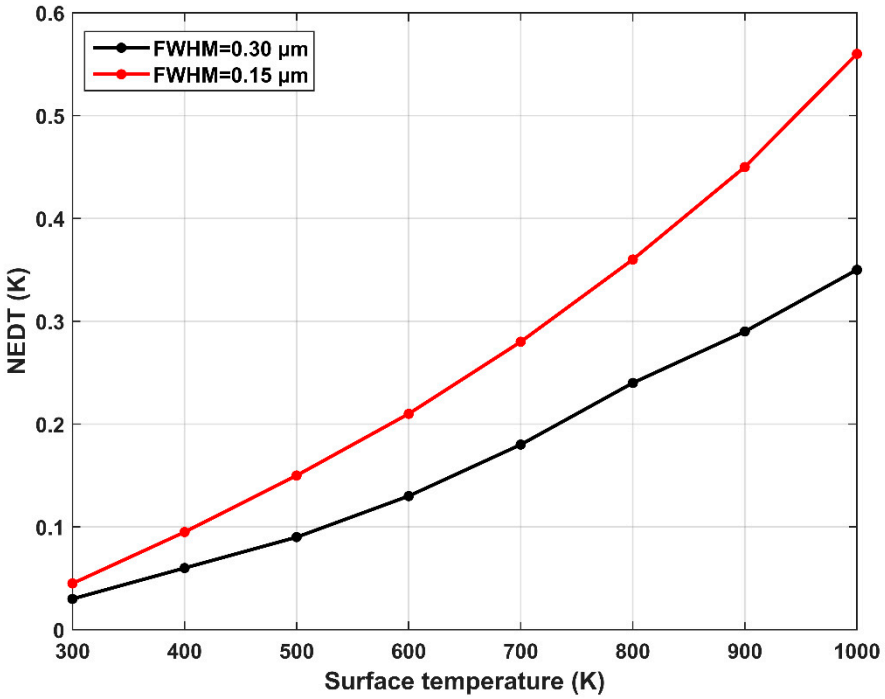

Figure 8. NEDT as function of surface temperature considering a response function with FWHM = 0.15 μm (red line) and FWHM = 0.30 μm (black line).

4. Discussion

The model simulation results highlighted the radiance difference to be appreciated from a multispectral space imaging sensor with the absorption band at 4.8 μm for CO_2 concentration starting from atmospheric background (400 ppm) to 1000 ppm. This difference has been transformed in a

NEDT (Table 2). The values of NEDT strongly depend on the ground temperature and the FWHM of the response function. Higher temperatures under emitting point sources induce NEDT higher values, allowing the possibility to retrieve CO_2 changes. Considering the current space instruments, the MWIR bands (4.4 μm and 4.5 μm) of the MODIS instrument on board Terra satellite have a NEDT of 0.25 K as the predicted was 0.15 K at 300 K [30]. Instead, the more recent MWIR channel 3.74 μm of AVHRR-3 on board the METOP satellites is 0.12 K at 300 K [31]. Taking into account also the TIR operational sensor ASTER (Advanced Spaceborne Thermal Emission and Reflection Radiometer) [32], the NEDT is ≤0.2 K at 300 K for the five thermal bands (8–11 μm). Moreover, considering the SNR of the actual SWIR bands of TANSO-FTS on board GOSAT-2 and the OCO-2 instrument of SNR > 300, the difference in sensitivity with our results (Table 2) is for a target surface at temperature values >400 K. This means that the sensitivity of 4.8 μm channel is satisfied for high-temperature events (>400K) by using the actual technologies.

From our results, in order to appreciate a CO_2 variation of 10 ppm and considering a surface at 300 K, the necessary NEDT is 0.045 K for a FWHM of 0.15 μm and 0.03 K for a FWHM of 0.30 μm. So, the required characteristics of a new space sensor employing the 4.8 μm channel, with a NEDT of about 0.045 K, are not so far from actual available technologies (e.g., AVHRR-3). Moreover, tests on the width of sensor response function give best results for the narrower one (0.15 μm). This NEDT is calculated for a 'cold' surface at standard condition (300 K). Instead, for a 'hot' surface >600 K, the NEDT result <0.21 K is completely compliant with the actual technologies for both FWHM.

Future space instruments should consider this wide range of values to retrieve CO_2 concentrations on point sources and also to avoid saturation problems that actually characterized the acquisition of high-temperature events. Instrument sensitivity as well as repeat cycles are expected to increase significantly in the near future with new technological solutions [25].

The possibility of detecting CO_2 point sources is related to both the sensitivity and the spatial resolution of the sensor itself.

5. Conclusions

In this work, MODTRAN simulations were focused on the CO_2 absorption band at 4.8 μm, in the MWIR spectral region. Model runs were performed for a set of surface temperatures, in the range 300–1000 K, with the aim to characterize the channel performance in the case of HTEs with emission of carbon dioxide. The at-sensor radiance sharply increases with increasing temperatures, ranging from 1 $Wm^{-2}sr^{-1}\mu m^{-1}$ (in the standard condition) to more than 1200 $Wm^{-2}sr^{-1}\mu m^{-1}$ (in the warmest case). Furthermore, the FWHM parameter is very important to detect changes in the gas concentration: two values (0.15 and 0.30 μm) are considered in the present paper. The narrower function leads to best challenges in order to detect gas emissions due to the highest values of NEDT calculated for this case. So, simulation results provide indications on the sensitivity necessary to appreciate carbon dioxide variations and then retrieve their concentrations from a space sensor. In this study, a variation of 10 ppm in gas concentration was considered as target; this value is equivalent to about 2 kg/m^2 more in the columnar abundance XCO_2. The values of NEDT closest to the actual technologies are obtained considering the FWHM equal to 0.15 μm in the range from 0.045 to 0.56 K depending on the ground temperature. The current operative spaceborne multispectral imaging space radiometers do not include the channel at 4.8 μm; however, sensors with MWIR channels as MODIS and AVHRR have a NEDT in the range 0.1–0.2 K. Considering our results, we can say that current space technology could be able to detect changes of tens ppm in CO_2 concentration for standard condition (at 300 K), and very little changes on HTEs emitting greenhouse gases.

In the framework of the studies addressed to the next generation of multispectral space sensors, this work represents a first step to understand the behavior of the considered CO_2 absorption band, less studied in the literature, and the possibility to include the 4.8 μm band in a new instrument dedicated to the Earth's observation.

Author Contributions: Methodology, V.R.; Writing-Review & Editing, C.S.; M.S.; M.F.B.; Supervision, V.R.; Project Administration, V.R.; Funding Acquisition, V.R. All authors have read and agreed to the published version of the manuscript.

Funding: This research was funded by the Agenzia Spaziale Italiana (ASI) through the contract n. 2018-17-HH.0 between ASI and the Istituto Nazionale di Geofisica e Vulcanologia (INGV).

Acknowledgments: This work was supported by the Agenzia Spaziale Italiana (ASI) in the framework of a joint study between ASI and NASA/JPL.

Conflicts of Interest: The author declares no conflict of interest.

References

1. Masson-Delmotte, V.; Zhai, P.; Pörtner, H.O.; Roberts, D.; Skea, J.; Shukla, P.R.; Pirani, A.; Moufouma-Okia, W.; Péan, C.; Pidcock, R.; et al. IPCC, 2018: Summary for Policymakers. In *Global Warming of 1.5 °C. An IPCC Special Report on the Impacts of Global Warming of 1.5 °C above Pre-Industrial Levels and Related Global Greenhouse Gas Emission Pathways, in the Context of Strengthening the Global Response to the Threat of Climate Change, Sustainable Development, and Efforts to Eradicate Poverty*; World Meteorological Organization: Geneva, Switzerland, 2018; p. 32.
2. Arneth, A.; Barbosa, H.; Benton, T.; Calvin, K.; Calvo, E.; Connors, S.; Cowie, A.; Davin, E.; Denton, F.; van Diemen, R.; et al. IPCC, 2019: Summary for Policymakers. In *An IPCC Special Report on Climate Change, Desertification, Land Degradation, Sustainable Land Management, Food Security, and Greenhouse Gas Fluxes in Terrestrial Ecosystems*; World Meteorological Organization: Geneva, Switzerland, 2019; approved draft.
3. Chédin, A.; Saunders, R.; Hollingsworth, A.; Scott, N.; Matricardi, M.; Etcheto, J.; Clerbaux, C.; Armante, R.; Crevoisier, C. The feasibility of monitoring CO_2 from high-resolution infrared sounders. *J. Geophys. Res.* **2003**, *108*, 4064. [CrossRef]
4. Chédin, A.; Serrar, S.; Scott, N.A.; Crevoisier, C.; Armante, R. First global measurement of midtropospheric CO_2 from NOAA polar satellites: Tropical zone. *J. Geophys. Res.* **2003**, *108*, 4581. [CrossRef]
5. Chevallier, F.; Fisher, M.; Peylin, P.; Serrar, S.; Bousquet, P.; Bréon, F.M.; Chédin, A.; Ciais, P. Inferring CO_2 sources and sinks from satellite observations: Method and application to TOVS data. *J. Geophys. Res.* **2005**, *110*, D24309. [CrossRef]
6. Engelen, R.J.; Serrar, S.; Chevallier, F. Four dimensional data assimilation of atmospheric CO_2 using AIRS observations. *J. Geophys. Res.* **2009**, *114*, D03303. [CrossRef]
7. Crevoisier, C.; Chédin, A.; Matsueda, H.; Machida, T.; Armante, R.; Scott, N.A. First year of upper tropospheric integrated content of CO_2 from IASI hyperspectral infrared observations. *Atmos. Chem. Phys.* **2009**, *9*, 4797–4810. [CrossRef]
8. Hilton, F.R.; Armante, T.; August, C.; Barnet, A.; Bouchard, C.; Camy-Peyret, V.; Capelle, L.; Clarisse, C.; Clerbaux, P.; Coheur, A.; et al. Hyperspectral Earth Observation from IASI: Five Years of Accomplishments. *Bull. Amer. Meteor. Soc.* **2012**, *93*, 347–370. [CrossRef]
9. Serio, C.; Masiello, G.; Camy-Peyret, C.; Liuzzi, G. CO_2 spectroscopy and forward/inverse radiative transfer modelling in the thermal band using IASI spectra. *J. Quant. Spectrosc. Radiat. Transf.* **2019**, *222–223*, 65–83. [CrossRef]
10. Buchwitz, M.; de Beek, R.; Burrows, J.P.; Bovensmann, H.; Warneke, T.; Notholt, J.; Meirink, J.F.; Goede, A.P.H.; Bergamaschi, P.; Korner, S.; et al. Atmospheric methane and carbon dioxide from SCIAMACHY satellite data: Initial comparison with chemistry and transport models. *Atmos. Chem. Phys.* **2005**, *5*, 941–962. [CrossRef]
11. Kuze, A.; Suto, H.; Nakajima, M.; Hamazaki, T. Thermal and near infrared sensor for carbon observation Fourier-transform spectrometer on the Greenhouse Gases Observing Satellite for greenhouse gases monitoring. *Appl. Opt.* **2009**, *48*, 6716–6733. [CrossRef]
12. Frankenberg, C.; Pollock, R.; Lee, R.A.M.; Rosenberg, R.; Blavier, J.F.; Crisp, D.; O'Dell, C.W.; Osterman, G.B.; Roehl, C.; Wennberg, P.O.; et al. The Orbiting Carbon Observatory (OCO-2): Spectrometer performance evaluation using pre-launch direct sun measurements. *Atmos. Meas. Tech.* **2015**, *8*, 301–313. [CrossRef]
13. Miller, S.M.; Michalak, A.M.; Yadav, V.; Tadić, J.M. Characterizing biospheric carbon balance using CO_2 observations from the OCO-2 satellite. *Atmos. Chem. Phys.* **2018**, *18*, 6785–6799. [CrossRef]
14. Orbiting Carbon Observatory-2 (OCO-2). Available online: https://ocov2.jpl.nasa.gov/index.cfm (accessed on 23 October 2019).

15. Yang, D.; Liu, Y.; Cai, Z.; Chen, X.; Yao, L.; Lu, D. First Global Carbon Dioxide Maps Produced from TanSat Measurements. *Adv. Atmos. Sci.* **2018**, *35*, 621. [CrossRef]
16. Eldering, A.; Taylor, T.E.; O'Dell, C.W.; Pavlick, R. The OCO-3 mission: Measurement objectives and expected performance based on 1 year of simulated data. *Atmos. Meas. Tech.* **2019**, *12*, 2341–2370. [CrossRef]
17. Schwandner, F.M.; Gunson, M.R.; Miller, C.E.; Carn, S.A.; Eldering, A.; Krings, T.; Verhulst, K.R.; Schimel, D.S.; Nguyen, H.M.; Crisp, D.; et al. Spaceborne detection of localized carbon dioxide sources. *Science* **2017**, *358*, eaam5782. [CrossRef]
18. Tanaka, T.; Fukabori, M.; Sugita, T.; Nakajima, H.; Yokota, T.; Watanabe, T.; Sasano, Y. Spectral line parameters for CO_2 bands in the 4.8-to 5.3-μm region. *J. Mol. Spectrosc.* **2006**, *239*, 1–10. [CrossRef]
19. Lombardo, V.; Harris, A.J.L.; Calvari, S.; Buongiorno, M.F. Spatial variations in lava flow field thermal structure and effusion rate derived from very high spatial resolution hyperspectral (MIVIS) data. *J. Geophys. Res. Solid Earth* **2009**, *114*. [CrossRef]
20. Spinetti, C.; Carrere, V.; Buongiorno, M.F.; Sutton, A.J.; Elias, T. Carbon Dioxide of Kilauea Volcanic Plume Retrieved by Means of Airborne Hyperspectral Remote Sensing. *Remote Sens. Environ.* **2008**, *112*, 3192–3199. [CrossRef]
21. Heymann, J.; Reuter, M.; Buchwitz, M.; Schneising, O.; Bovensmann, H.; Burrows, J.P.; Massart, S.; Kaiser, J.W.; Crisp, D.; O'Dell, C.W. CO_2 emission of Indonesian fires in 2015 estimated from satellite-derived atmospheric CO_2 concentrations. *Geophys. Res. Lett.* **2017**, *44*, 1537–1544. [CrossRef]
22. Nassar, R.; Hill, T.G.; McLinden, C.A.; Wunch, D.; Jones, B.A.; Crisp, D. Quantifying CO_2 emissions from individual power plants from space. *Geophys. Res. Lett.* **2017**, *44*. [CrossRef]
23. Griffin, M.K.; Burke, H.K.; Kerekes, J.P. Understanding radiative transfer in the midwave infrared, a precursor to full spectrum atmospheric compensation. In *Algorithms and Technologies for Multispectral, Hyperspectral, and Ultraspectral Imagery X*; International Society for Optics and Photonics: Bellingham, WA, USA, 2004; Volume 5425, pp. 348–356.
24. MODTRAN Computer Code. Available online: http://modtran.spectral.com/ (accessed on 23 October 2019).
25. Queißer, M.; Burton, M.; Kazahaya, R. Insights into geological processes with CO_2 remote sensing–A review of technology and applications. *Earth Sci. Rev.* **2019**, *188*, 389–426. [CrossRef]
26. Spinetti, C.; Mazzarini, F.; Casacchia, R.; Colini, L.; Neri, M.; Behncke, B.; Pareschi, M.T. Spectral properties of volcanic materials from hyperspectral field and satellite data compared with LiDAR data at Mt. Etna. *Int. J. Appl. Earth Obs. Geoinf.* **2009**, *11*, 142–155. [CrossRef]
27. Hook, S.J.; Myers, J.J.; Thome, K.J.; Fitzgerald, M.; Kahle, A.B. The MODIS/ASTER airborne simulator (MASTER)—A new instrument for earth science studies. *Remote Sens. Environ.* **2001**, *76*, 93–102. [CrossRef]
28. MASTER Airborne Simulator. Available online: https://master.jpl.nasa.gov/ (accessed on 23 October 2019).
29. Hodgkinson, J.; Smith, R.; On Ho, W.; Saffell, J.R.; Tatam, R.P. Non-dispersive infra-red (NDIR) measurement of carbon dioxide at 4.2 μm in a compact and optically efficient sensor. *Sens. Actuators B Chem.* **2013**, *186*, 580–588. [CrossRef]
30. Xiong, X.; Wu, A.; Chen, N.; Chiang, K.; Xiong, S.; Wenny, B.; Barnes, W.L. Detector noise characterization and performance of MODIS thermal emissive bands. In *Earth Observing Systems XII*; International Society for Optics and Photonics: Bellingham, WA, USA, 2007; Volume 6677. [CrossRef]
31. Rosenfeld, D.; Cattani, E.; Melani, S.; Levizzani, V. Considerations on daylight operation of 1.6-VERSUS 3.7-μM channel on NOAA and Metop satellites. *Bull. Amer. Meteor. Soc.* **2004**, *85*, 873–882. [CrossRef]
32. ASTER Space Mission. Available online: https://asterweb.jpl.nasa.gov/ (accessed on 23 October 2019).